

15 μm cut-off 128 x 128 quantum well infrared photodetectors (QWIPs) camera

G. Sarusi*, S. D. Gunapala, J. S. Park, J. K. Liu, T. L. Lin**, P. D. Maker, R. E. Muller, and B. F. Levine⁺

Center for Space Microelectronics Technology, Jet Propulsion Laboratory, California Institute of Technology, Pasadena, CA 91109

* elop-Electroptics Industries Ltd., Rehovot 76111 Israel

** Siliconix, Santa Clara, CA 95056

+ AT&T Bell Laboratories, Murray Hill, NJ 07974

ABSTRACT

We discuss the development and the performances of a very long wavelength (13.5 - 15 μm) 128x128 AlGaAs/GaAs multiquantum well infrared imaging, system. Highly uniform, high-yield QWIP focal plane array was hybridized to a CMOS multiplexer operating in a direct injection mode. For efficient light coupling an integral random scattering reflector (Random Grating) was incorporated. Due to the high uniformity, excellent imagery, low noise as well as a noise equivalent temperature difference (NEAT) of less than 30 mK were obtained when operating around 45 K. Therefore, high image contrast signal to noise ratio has been achieved.

2. INTRODUCTION

We have developed a first generation 15 μm GaAs/Al_xGa_{1-x}As 128x128 quantum well infrared photodetectors (QWIPs) focal plane array (FPA) for a staring infrared (IR) sensor system. There are several applications that require very long wavelength, large, uniform, reproducible, low cost, low 1/f noise, low power dissipation, and radiation hard IR FPAs. For example, the absorption lines of many gas molecules, such as ozone, water, carbon monoxide, carbon dioxide, and nitrous oxide occur in the wavelength region from 3 to 18 μm . Thus, IR imaging systems that operate in the very long wavelength IR (VWIR) region (12 - 18 μm) are also required in many space applications such as monitoring the global atmospheric temperature profiles, relative humidity profiles, cloud characteristics, and the distribution of minor constituents in the atmosphere which are being planned for the NASA's Earth Observing System¹. The GaAs based QWIP^{2,3,4} is a potential candidate for space borne applications and it can meet all of the requirements mentioned above for this spectral region.

Fig. 1 shows the schematic conduction band diagram of a typical *bound-to-continuum* QWIP⁵ which utilize bound-to-continuum intersubband absorption. By carefully designing the quantum well

structure, as well as the light coupling to the detector, it is possible to optimize the material to have an optical response in the desired spectral range and determine the spectral response shape⁶. In QWIPs, the dark current originates from three different mechanisms⁷. The first process is due to quantum mechanical tunneling from well to well through the $\text{Al}_x\text{Ga}_{1-x}\text{As}$ barriers (sequential tunneling). This process is independent of temperature. Sequential tunneling dominates the dark current at very low temperatures (<30 K for 15 μm QWLPS). The second mechanism is thermally assisted tunneling which involves a thermal excitation and tunneling through the tip of the barrier into the continuum energy levels. This process governs the dark current at medium temperatures. The third mechanism is classical thermionic emission and it dominates the dark current at higher temperatures (>45 K for 15 μm QWIPs). Consequently, for QWIPs operating at higher temperatures the last mechanism is the major source of dark current⁷.

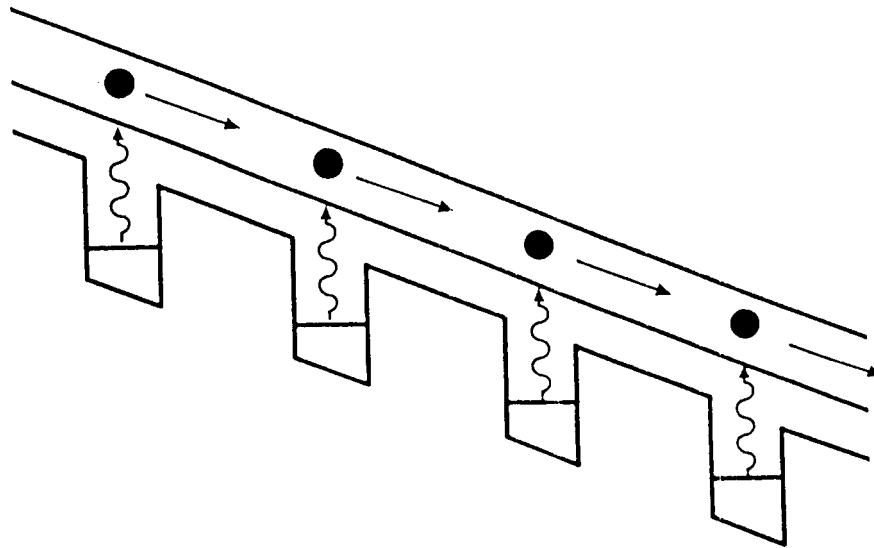


Fig. 1 Schematic diagram of the conduction band in a bound-to-continuum QWIP with an electric field. Absorption of IR photons can photo excite electrons from the ground state of the quantum well into the continuum, causing a photocurrent.

3. EXPERIMENT

The device structure consist of 50 periods containing 65 \AA wells of GaAs (doped $n = 2 \times 10^{17} \text{ cm}^{-3}$), and 600 \AA barriers of $\text{Al}_{0.15}\text{Ga}_{0.85}\text{As}$ (sandwiched between 0.5 μm GaAs top and bottom contact layers doped $n = 2 \times 10^{17} \text{ cm}^{-3}$) grown on a semi-insulating GaAs substrate by molecular beam epitaxy (MBE). Then 1.1 μm thick GaAs cap layer on top of 300 \AA $\text{Al}_{0.15}\text{Ga}_{0.85}\text{As}$ stop-etch layer was grown *in situ* on top of the device structure to fabricate the light coupling optical cavity. MBE grown QWIP structure was processed into 200 μm diameter mesa test structures (area = $3.14 \times 10^{-4} \text{ cm}^2$) using wet chemical etching and Au/Ge ohmic contacts were evaporated onto the top and bottom contact layers.

The dark current-voltage curves of the QWIP was measured as a function of temperature from $T = 30\text{-}55$ K and the curves are shown in Fig. 2. The asymmetry in the dark current is attributed to the Si dopant migration into the growth direction⁸ and hence higher asymmetry in the band structure.

The responsivity spectra of these detectors were measured using a 1000 K blackbody source and a grating monochromator. The absolute peak responsivities (R_p) of the detectors were measured using a calibrated blackbody source. The detector were back illuminated through a 45° polished facet⁶ and its responsivity spectrum is shown in Fig. 3. The responsivity of the detector peak at $14.2\ \mu\text{m}$ and the peak responsivity (R_p) of the detector is $420\ \text{mA/W}$. The spectral width and the cutoff wavelength are $\Delta\lambda/\lambda = 13\%$ and $\lambda_c = 14.9\ \mu\text{m}$. The bias dependent peak responsivity of the detector is shown in Fig. 4. The measured absolute responsivity of the detector is small up to about $V_B = 1\ \text{V}$. Beyond that it increases nearly linearly with the bias reaching $R_p = 560\ \text{mA/W}$ at $V_B = 4\ \text{V}$. This type of behavior of responsivity versus bias is typical for a bound-to-quasibound QWIP. The peak quantum efficiency was 3% (lower quantum efficiency is due to the lower well doping density) for a 45° double pass.

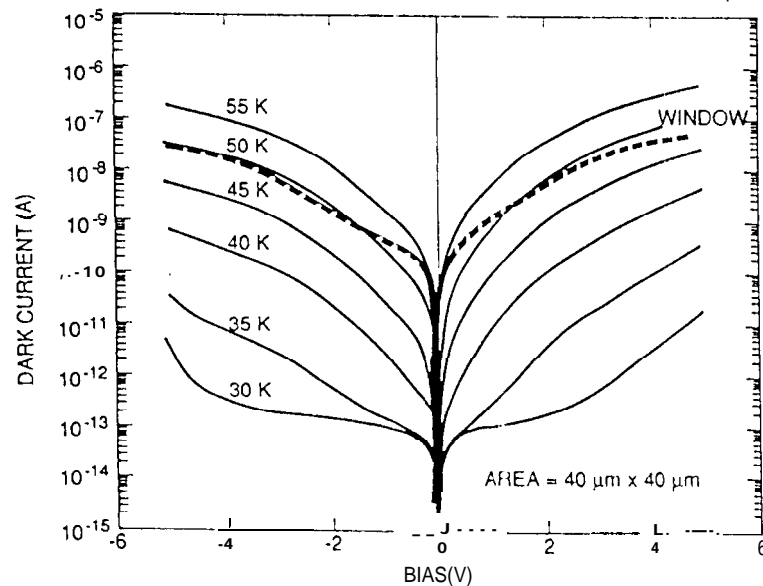


Fig. 2 Dark current of $40 \times 40\ \mu\text{m}^2$ QWIP pixel ($\lambda_c = 14.9\ \mu\text{m}$) as a function of bias voltage at various temperatures.

The current noise in was measured using a spectrum analyzer and experimentally 'determined the photoconductive gain⁹ g using $g = i_n^2 / 4eI_D B + 1/2N$, where B is the measurement band width and N is the number of quantum wells. Photoconductive gain of the detector reached 0.32 at $V_B = -6\ \text{V}$. Since the gain of QWIP is inversely proportional to the number of quantum wells N , the better comparison would be the well capture probability p_c , which is directly related to the gain⁹ by $g = 1/Np_c$. The calculated

well capture probabilities are 20% at low bias and 6% at high bias voltage which indicate the excellent hot-electron transport in this device structure. The peak defectivity is defined as $D_p^* = R_p \sqrt{AB} / i_n$, where R_p is the peak responsivity, A is the area of the detector and $A = 3.14 \times 10^{-4} \text{ cm}^2$. The measured peak defectivity at bias $V_B = -3 \text{ V}$ and temperature $T = 55 \text{ K}$ is $1.6 \times 10^{10} \text{ cm}^2/\sqrt{\text{Hz/W}}$.

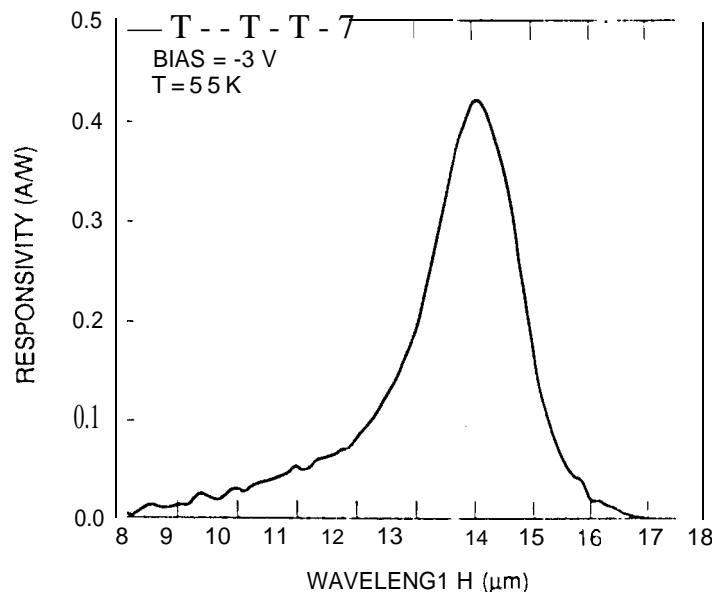


Fig. 3 Responsivity spectra of bound-to-quasicontinuum VWIR QWIP focal plane array sample at temperature $T = 55 \text{ K}$. The spectral response peak at $14.2 \mu\text{m}$ and the long wavelength cutoff is at $14.9 \mu\text{m}$.

4. LIGHT COUPLING

Many more passes of IR light inside the detector structure can be obtained by incorporating a randomly roughened reflecting surface on top of the detectors which also remove the light coupling limitations and make two dimensional QWIP imaging arrays feasible. A factor of eight enhancement in QWIP responsivity compared to 45° illumination geometry has been achieved with a randomly roughened reflecting surface¹⁰. The random structure on top of the detector prevents the light from being diffracted normally backward after the second bounce as happens in the case of cross-grating. After each bounce, light is scattered at a different random angle and the only chance for light to escape out of the detector is when it is reflected towards the surface within the critical angle of the normal. For the GaAs/air interface this angle is about 17° , defining a very narrow escape cone for the trapped light. The reflector was designed with two levels of scattering surfaces located at quarter wavelength separations. The area of the top unetched level is equal to the area of the etched level ($\lambda/4$ deep). Therefore, the normally reflected light intensities from the top and bottom surfaces of random reflector are equal and 180° out of phase, thus maximizing the destructive interference at normal reflection and

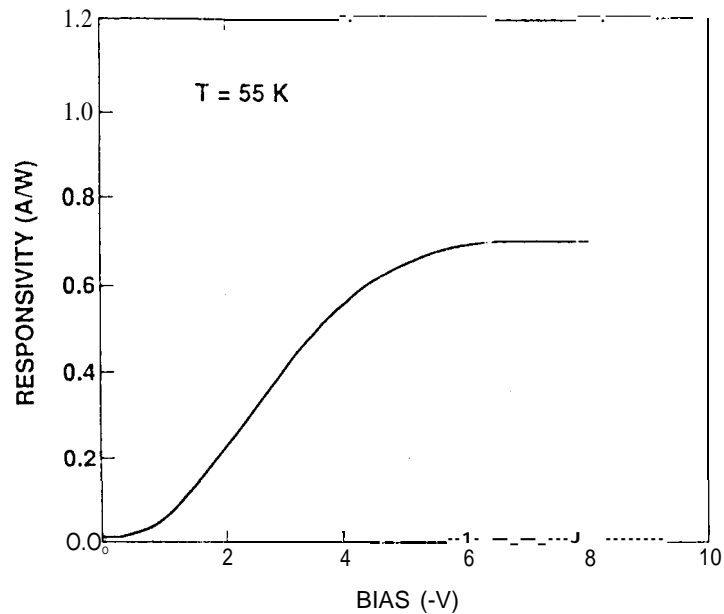


Fig. 4 Peak responsivity as a function of bias voltage at temperature $T = 55$ K.

hence lower the light leakage through the escape cone. This random structure was fabricated on the detectors by using standard photolithography and CCl_2F_2 selective dry etching. The advantage of the photolithographic process over a completely random process is the ability to accurately control the feature size and to preserve the pixel to pixel uniformity which is a prerequisite for high sensitivity imaging focal plane arrays.

5. IMAGING

The photoconductive QWIPS of the 128×128 FPAs were then fabricated by wet chemical etching through the photosensitive $\text{GaAs}/\text{Al}_x\text{Ga}_{1-x}\text{As}$ multi quantum well layers into the $0.5 \mu\text{m}$ thick doped GaAs contact layer. Figure 5 shows an expanded corner of 128×128 QWIP FPA. The pitch of the FPA is $50 \mu\text{m}$ and the actual pixel size is $38 \times 38 \mu\text{m}^2$. Then the random reflectors on the top of the detectors were covered with Au/Ge and Au for Ohmic contact and reflection, Then iridium bumps were evaporated on top of the detectors for Si read out circuit (ROC) hybridization. A single QWIP FPA was chosen (cutoff wavelength of this sample is $14.9 \mu\text{m}$) and bonded to a 128×128 Si multiplexer (Amber AE-159) and biased at $V_b = -2.7$ V. The FPA was back-illuminated through the flat thinned substrate (thickness $\approx 25 \mu\text{m}$). This initial array gave excellent images with 99.9% of the pixels working, demonstrating the high yield of GaAs technology. An excellent uncorrected photocurrent uniformity has been achieved with standard deviation of only $\sigma = 2.4\%$. The uniformity after correction was 0.2%. As

mentioned earlier this high yield is due to the excellent GaAs growth uniformity and the mature GaAs processing technology.

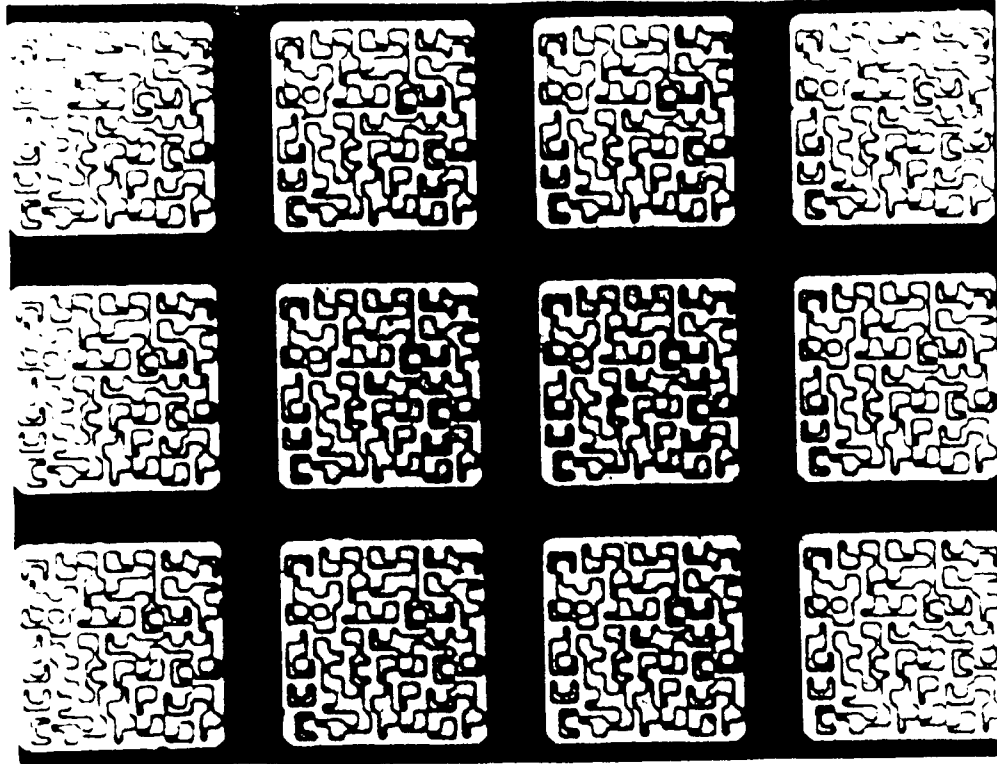


Fig. 5 Expanded corner of 128x128 QWIP FPA shows two level random reflectors on individual QWIP pixels ($38 \times 38 \mu\text{m}^2$). The random reflectors increase the light coupling efficiency by factor of eight when the substrate thin down to $\sim 1 \mu\text{m}$

Video images were taken at various frame rates varying from 50 to 200 Hz with f/2.3 KRS-5 optics at temperatures as high as $T = 45 \text{ K}$, using a ROC capacitor having a charge capacity of 4×10^7 electrons. Fig. 6 shows an image of a truck with $\text{NEAT} = 30 \text{ mK}$. The warm tires, motor, and the driver's cabin can clearly be seen. The measured noise equivalent temperature difference NEAT of the FPA was 30 mK at an operating temperature of $T = 45 \text{ K}$ for 300 K background. This reasonably agrees with our calculated value of 10 mK. We have used the following equation to calculate the NEAT of the FPA.

$$\text{NEAT} = \frac{\sqrt{AB}}{D_B^* (dP_B / dT)}$$

Where D_B^* is the blackbody defectivity and dP_B / dT is the derivative of the integrated blackbody power with respect to temperature. No band pass filters were used and it is unnecessary in QWIP camera systems, because of the narrow spectral response of QWIPs. It should be noted that these initial



Fig. 6 One frame from a $15\mu\text{m}$ QWIP video image of a truck with $\text{NE}\Delta\text{T} = 30\text{ mK}$. The warm tires, motor, and the driver's cabin can be clearly seen.

unoptimized FPA results are far from optimum. The QWIP device structures was not optimized; the gratings were also not optimized for the maximum light coupling efficiency; no microlenses were used; no antireflection coatings were used; substrate was not thinned enough (the hybrid was thinned to 25 μm , however, it was not sufficient to improve the light coupling efficiency to small pixel and in fact this explains the slightly higher measured $\text{NE}\Delta\text{T}$); and finally the multiplexer used was a photovoltaic InSb multiplexer which is certainly not optimized to supply the proper bias and impedance levels required by photoconductive QWIPs. Implementation of these improvements should significantly enhance the QWIP focal plane array operating temperatures (i.e., 77 K for 10 μm and 55 K for 15 μm).

6. ACKNOWLEDGMENTS

We are grateful to C. A. Kukkonen, V. Sarohia, S. K. Khanna, K. M. Koliwad, B. A. Wilson, and P. J. Grunthaner of the Jet Propulsion Laboratory for encouragement and support of this work. The

research described in this paper was performed by the Center for Space Microelectronics Technology, Jet Propulsion Laboratory, California Institute of Technology. and was jointly sponsored by the Ballistic Missile Defense Organization/Innovative Science and Technology Office, and the National Aeronautics and Space Administration, Office of Advanced Concepts and Technology.

7. REFERENCES

1. M. T. Chahine, "Sensor requirements for Earth and Planetary observations," *Proceedings of Innovative Long Wavelength Infrared Detector Workshop*, Pasadena, California, pp. 3-31, April 24-26, 1990.
2. C. G. Bethea, B. F. Levine, M. T. Asom, R. E. Leibenguth, J. W. Stayt, K. G. Glogovsky, R. A. Morgan, J. D. Blackwell, and W. J. Parrish, "Long Wavelength Infrared 128 x 128 Al_xGa_{1-x}As/GaAs Quantum Well Infrared Camera and Imaging System," *IEEE Trans. Electron. Devices*, vol. 40, pp. 1957-1963, 1993.
3. L. J. Kozlowski, G. M. Williams, G. J. Sullivan, C. W. Farley, R. J. Andersson, J. Chen, D. T. Cheung, W. E. Tennant, and R. E. DeWames, "LWIR 128x128 GaAs/AlGaAs Multiple Quantum Well Hybrid Focal Plane Array," *IEEE Trans. Electron. Devices*, vol. ED-38, pp. 1124-1130, 1991.
4. W. A. Beck, T. S. Faska, J. W. Little, J. Albritton, and M. Sensiper, *Proceedings of the Second International Symposium on 2-20 μm Wavelength infrared Detectors and Arrays: Physics and Applications*, October 10-12, 1994, Miami Beach, Florida.
5. B. F. Levine, C. G. Bethea, G. Hasnain, V. O. Shen, E. Pelve, R. R. Abbott, and S. J. Hsieh, "High sensitivity low dark current 10 μm GaAs quantum well infrared photodetectors", *Appl. Phys. Lett.*, vol. 56, pp 851-853, 1990.
6. B. F. Levine, "Quantum Well Infrared Photodetectors", *J. Appl. Phys.*, vol. 74, pp R1-R81, 1993.
7. Sarath Gunapala, Gabby Sarusi, Jin Park, True-Lon Lin, and Barry Levine, "Infrared Detectors Reach New Lengths", *Physics World*, pp 35-40, December 1994.
8. H. C. Liu, Z. R. Wasilewski, and M. Buchanan, "Segregation of Si doping in GaAs-AlGaAs quantum wells and the cause of the asymmetry in the current-voltage characteristics of intersubband infrared detectors", *Appl. Phys. Lett.* vol. 63, pp 761-763, 1993.

9. W. A. Beck, "Photoconductive gain and generation-recombination noise in multiple-quantum-well infrared detectors", *Appl. Phys. Lett.*, vol. 63, pp 3589-3591, 1993.
10. G. Sarusi, B. F. Levine, S. J. Pearton, K. M. S. V. Bandara, and R. E. Leibenguth, "Improved performance of quantum well infrared photodetectors using random scattering optical coupling," *Appl. Phys. Lett.*, vol. 64, pp. 960-962, 1994.